ChemComm

Decorating an anisotropic Au_{13} core with dendron thiolates: enhancement of optical absorption and photoluminescence

Journal:	*ChemComm*
Manuscript ID	CC-COM-09-2021-005235.R1
Article Type:	Communication

COMMUNICATION

Decorating an anisotropic Au_{13} core with dendron thiolates: enhancement of optical absorption and photoluminescence

Tsubasa Omoda,[a] Shinjiro Takano,[a] Shinya Masuda[a] and Tatsuya Tsukuda*[a,b]

Received 00th January 20xx,
Accepted 00th January 20xx

DOI: 10.1039/x0xx00000x

We successfully introduced up to 12 poly(benzyl ether)dendron-thiols of the second generation (D2SH) into the Au_{13} core of $[Au_{23}(ScC_6H_{11})_{16}]^-$ while retaining the geometric structure. The decoration with D2SH enhanced the optical absorbance in the >2.5 eV region and the quantum yield of photoluminescence at ~1.6 eV by ~15 times.

Dendrons, which are composed of branching layers, each known as a 'generation' (G), with a functional group at the focal point, have been used for encapsulating metal nanoparticles (NPs).[1,2] The diameters of the metal NPs have been controlled as a function of G and it was found that the NPs became highly monodisperse at a certain G due to the packing of the wedge-like shaped dendrons.[3,4] The assembling nature of the NPs was also found to be dependent on G, and one-dimensional assembly has been reported.[5,6] An exposed surface could be designed on the NPs for catalysis by taking advantage of the steric repulsion between adjacent dendrons.[7] These examples demonstrate that the dendrons are attractive surfactants for metal NPs.

Thus, small gold clusters (<2 nm) modified with dendrons $Au_n(Den)_m$ may provide an interesting class of nanomaterials exhibiting novel size-specific properties. Their synthesis requires precise chemical compositions, because their physicochemical properties change drastically even by a difference in a single atom.[8,9] In addition, the geometric structures should be determined by single-crystal X-ray diffraction (SCXRD) to understand the origin of the novel properties.[10] However, their crystallization is a huge challenge due to the structural fluxionality of the branching layers. One method for overcoming this inherent problem is to introduce the dendrons to a preformed ligand (L)-protected Au cluster $Au_n(L)_m$ whose structure has been solved by SCXRD. The core motif can be monitored by optical absorption spectroscopy since the spectra for these small Au clusters are well structured and can be used as fingerprints.[11] Although the ligand exchange method has been applied for the synthesis of various monolayer protected Au clusters,[12-14] systematic synthesis of dendron-modified Au clusters has not yet been conducted, to our knowledge.

This study aimed to introduce dendrons to a well-defined Au cluster to tune their properties. The platform we chose was $[Au_{23}(SCy)_{16}]^-$ (CySH = cyclohexanethiol), having an anisotropic Au_{13} core with a face-centered cubic (FCC)-like motif (Fig. 1).[15] This anisotropic Au_{13} core is structurally frustrated by bulky and rigid CyS ligands with a secondary α-carbon (Scheme 1) and thus may undergo isomerization and/or reactions if the steric hindrance of the ligand layer around the Au_{13} core is released upon the introduction of dendrons. The photoluminescence quantum yield (PL QY) of $[Au_{23}(SCy)_{16}]^-$ (0.4% in CH_2Cl_2 solution)[16] may be enhanced if the core is rigidified through noncovalent interaction between the dendrons introduced. We used Fréchet-type dendron thiols of the first and second generation (D1SH and D2SH, Scheme 1).[17,18] The number of D*n*SH (*n* = 1, 2) introduced into $[Au_{23}(SCy)_{16}]^-$ was monitored by mass spectrometry. The core structure was examined by Au L_3-edge X-ray absorption fine structure (XAFS) spectroscopy. The optical and photophysical properties were studied as a function of the number and generation of D*n*SH ligands.

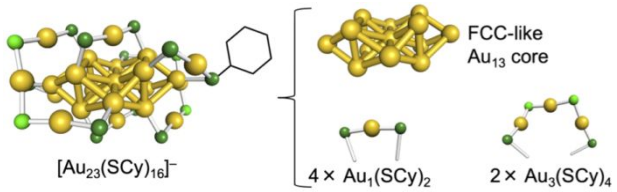

Fig. 1. Crystal structure (left) and anatomy representation (right) of $[Au_{23}(SCy)_{16}]^-$. Only one Cy group is shown for clarity. Color codes: yellow (Au); green and dark green (S).

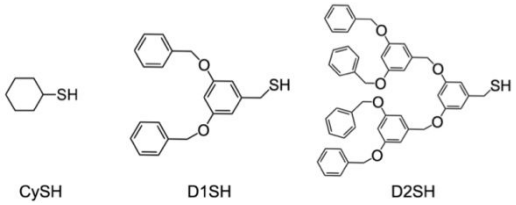

Scheme 1. Structures of CySH, D1SH, and D2SH.

[a] *Department of Chemistry, Graduate School of Science, The University of Tokyo, 7-3-1 Hongo, Bunkyo-ku, Tokyo 113-0033, Japan. Email: tsukuda@chem.s.u-tokyo.ac.jp*
[b] *Elements Strategy initiative for Catalysts and Batteries (ESICB), Kyoto University, Katsura, Kyoto 615-8520, Japan.*
†Electronic Supplementary Information (ESI) available: experimental details and supporting data. See DOI: 10.1039/x0xx00000x

Ligand-exchange reactions were conducted by adding D*n*SH to $[Au_{23}(SCy)_{16}](TOA)$ (TOA^+ = tetra-*n*-octylammonium cation) in CH_2Cl_2 at a molar ratio (MR) of 5, 20, 50, and 100 for n = 1 and MR = 5, 10, 20, 50, and 100 for n = 2. After the mixture was stirred for 6 h at 298 K, the molecular formulas of the products were determined by electrospray ionization (ESI) mass spectrometry. The ESI mass spectra of the products exhibited a series of mass peaks assignable to $[Au_{23}(SCy)_{16-k}(SD1)_k]^-$ (Fig. 2a) and $[Au_{23}(SCy)_{16-k}(SD2)_k]^-$ (Fig. 2b) with k = 1–16. The average number of D*n*S (n = 1, 2) introduced (x) was calculated as:

$$x = \frac{\sum_{k=0}^{16} kI_k}{\sum_{k=0}^{16} I_k}\#$$

where I_k is the intensity of the mass peaks of $[Au_{23}(SCy)_{16-k}(SDn)_k]^-$. The x values thus estimated are shown in Fig. 2a and 2b. Hereafter, the chemical composition of the products is described as $[Au_{23}(SCy)_{16-x}(SDn)_x]^-$. Fig. 2c plots the x values as a function of the MR of D*n*SH (n = 1, 2). The x values for both n = 1 and 2 increased similarly to the increase in the MR and reached a plateau of 10–12 (Fig. 2c). It was reported previously that ~13 CyS of $[Au_{23}(SCy)_{16}]^-$ could be replaced with 4-*tert*-butylbenzenethiol at 353 K.[19] These results imply that the maximum number of CyS replaceable in $[Au_{23}(SCy)_{16}]^-$ is not dependent on the structures of the incoming thiols. Previous experimental and theoretical studies on the ligand exchange of $MAu_{24}(SR)_{18}$ (M = Pd, Au) proposed that the RS ligands directly anchored on the Au core were preferentially replaced.[20-22] Since the maximal numbers of D*n*S introduced (10–12) were comparable to the number of anchoring CyS ligands (12) in $[Au_{23}(SCy)_{16}]^-$ (colored in dark green in Fig. 1), it is concluded that the CyS ligands directly bonded to the Au_{13} core of $[Au_{23}(SCy)_{16}]^-$ are preferentially replaced with D*n*SH regardless of their generation.

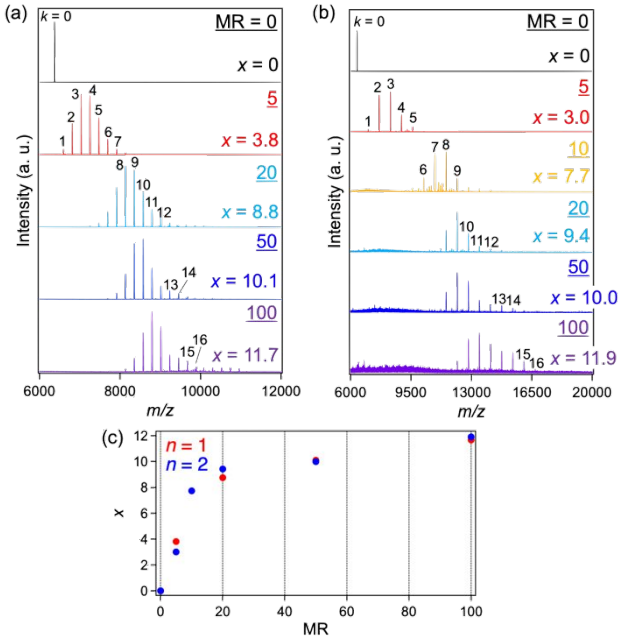

Fig. 2. ESI mass spectra of ligand-exchange products $[Au_{23}(SCy)_{16-k}(SDn)_k]^-$ as a function of the molar ratio (MR) of D*n*SH with respect to $[Au_{23}(SCy)_{16}]^-$: n = (a) 1 and (b) 2. The average numbers of D*n*S introduced (x) are shown. (c) Plots of the x values as a function of the MR for n =1 and 2.

Electronic and geometric structures of the Au_{13} cores of $[Au_{23}(SCy)_{16-x}(SDn)_x]^-$ (n = 1, 2) were monitored by optical spectroscopy. Fig. 3 shows the UV-visible (UV-vis) absorption spectra of $[Au_{23}(SCy)_{16-x}(SDn)_x]^-$ together with those of D*n*SH (n = 1, 2). The humps at ~4.4 eV observed in the spectra of $[Au_{23}(SCy)_{16-x}(SDn)_x]^-$ are assigned to the local excitation of the D*n*S ligands. In Fig. 3a, a new peak appeared at ~1.5 eV for $[Au_{23}(SCy)_{4.3}(SD1)_{11.7}]^-$ with $x \geq 8.8$, suggesting the concurrent formation of Au clusters with a different size and/or structure by the introduction of D1SH at MR ≥ 20. Our preliminary gel permeation chromatography and ESI mass analysis (Figs. S2 and S3) of the sample containing $[Au_{23}(SCy)_{4.3}(SD1)_{11.7}]^-$ suggest that the peak at ~1.5 eV in Fig. 3a is assigned to large Au_n clusters (n = 41–46) protected by mixed ligands. These results indicate that the introduction of D1SH into $[Au_{23}(SCy)_{16}]^-$ induced the fusion into larger Au clusters. On the other hand, the spectral profiles of $[Au_{23}(SCy)_{16-x}(SD2)_x]^-$, especially in the onset region (<2.5 eV), are nearly identical to that of $[Au_{23}(SCy)_{16}]^-$ (Fig. 3b). This result indicates that the Au_{13} core in $[Au_{23}(SCy)_{16-x}(SD2)_x]^-$ retained the original geometry since this onset band is assigned to the HOMO–LUMO transition of the core.[15] In contrast, the absorbance in the high energy region of >2.5 eV is gradually enhanced with x. This enhancement is ascribed to the involvement of charge transfer transitions between the Au_{13} core and D2S ligand layers bearing a large number of the phenyl groups.[23-25]

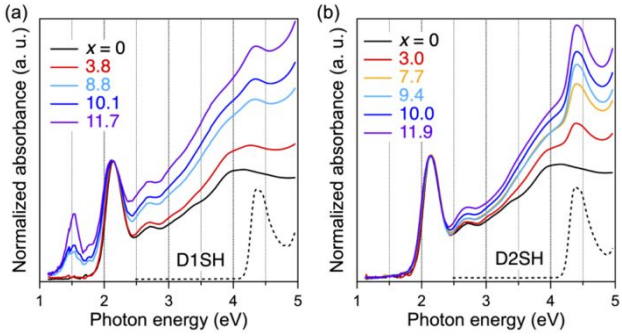

Fig. 3. UV-vis absorption spectra of ligand-exchange products of $[Au_{23}(SCy)_{16-x}(SDn)_x]^-$ with n = (a) 1 and (b) 2. The spectra are normalized by the absorbance at 2.14 eV. The dashed lines in (a) and (b) represent the absorption spectra of D1SH and D2SH, respectively.

To gain further structural information during the ligand exchange, Au L_3-edge XAFS spectra of $[Au_{23}(SCy)_{4.1}(SD2)_{11.9}]^-$ and $[Au_{23}(SCy)_{16}]^-$ were recorded at 10 K and compared. Both the X-ray absorption near-edge structure (XANES) spectra and extended X-ray absorption fine structure (EXAFS) oscillations of $[Au_{23}(SCy)_{4.1}(SD2)_{11.9}]^-$ were similar to those of $[Au_{23}(SCy)_{16}]^-$ (Figs. 4a and 4b). Curve fitting analysis on the Fourier-transformed (FT)-EXAFS spectrum of $[Au_{23}(SCy)_{4.1}(SD2)_{11.9}]^-$ was also conducted assuming the Au–S bond and Au–Au bonds with different lengths as reported previously.[26,27] The coordination numbers and bond lengths of $[Au_{23}(SCy)_{4.1}(SD2)_{11.9}]^-$ obtained by the curve fitting analysis quantitatively agreed with those of $[Au_{23}(SCy)_{16}]^-$ determined by the SCXRD (Table S2).[15] The longer (2.941±0.015 Å) and shorter (2.711±0.005 Å) Au–Au bonds were mainly distributed on the surface and inside of the Au_{13} core, respectively.[15] These results provide evidence that the geometric structures of the Au–Au and Au–S frameworks in $[Au_{23}(SCy)_{16}]^-$ did not change upon the introduction of D2SH, which is in sharp contrast to the case of D1SH. It is considered that CH–π/π–π interaction between benzyloxy groups in the D2S layer compensated for the steric effect of the CyS ligands near the Au_{13} core.

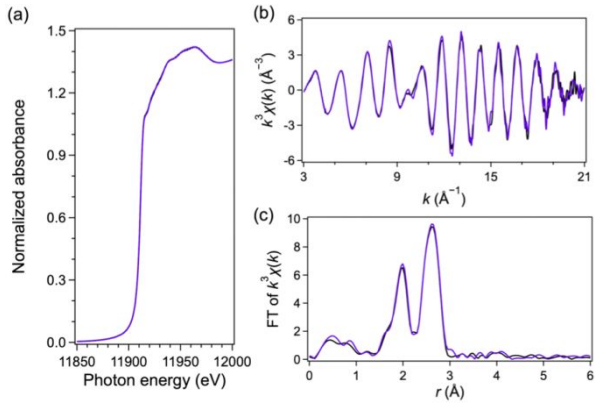

Fig. 4. Au L_3-edge (a) XANES spectra, (b) EXAFS oscillations, and (c) FT-EXAFS spectra of $[Au_{23}(SCy)_{4.1}(SD2)_{11.9}]^-$ (purple) and $[Au_{23}(SCy)_{16}]^-$ (black).

Lastly, we investigated the effects of the D*n*S ligands on the PL properties of $[Au_{23}(SCy)_{16}]^-$. Fig. S4 shows the PL spectra and PL decay profiles of $[Au_{23}(SCy)_{16}]^-$ in deaerated toluene. The PL QY was estimated to be 0.3% by using a dye standard,[28] slightly smaller than that previously reported (0.4% in CH_2Cl_2 solution).[16] The decay curve of the PL intensity $I(t)$ could not be fitted by a single component, but by two components[16] expressed as follows:

$$I(t) = A_1\exp\left(-\frac{t}{\tau_1}\right) + A_2\exp\left(-\frac{t}{\tau_2}\right)\#$$

where A_i and τ_i (i = 1, 2) are pre-exponential factors and lifetimes, respectively. The two emissions with lifetimes of 21 and 89 ns were tentatively assigned to the fluorescence and phosphorescence, respectively, since the latter component was almost completely quenched after bubbling with O_2 (Fig. S4, Table S3). Similar PL profiles in the presence and absence of O_2 (Fig. S4a) suggest that the fluorescence and phosphorescence spectra exhibited similar profiles.

Here we discuss the effect of D2S on the PL properties of $[Au_{23}(SCy)_{16}]^-$. Fig. 5a shows the x-dependent PL spectra of $[Au_{23}(SCy)_{16-x}(SD2)_x]^-$ excited at 2.16 eV in toluene. The

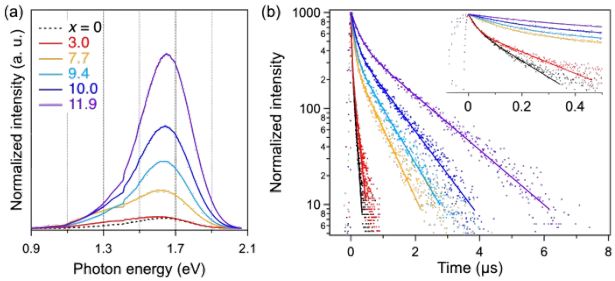

Fig 5. (a) PL spectra and (b) logarithm plots of PL decay of $[Au_{23}(SCy)_{16-x}(SD2)_x]^-$ in toluene. The spectra in (a) are normalized by the absorbance at the excitation energy (2.16 eV). The inset of (b) shows its enlarged view. The solid lines in (b) are fitted results.

Table 1. Summary of photophysical properties of $[Au_{23}(SCy)_{16-x}(SD2)_x]^-$.

x	PL QY (%)	$A_1/(A_1+A_2)$ (%)	τ_1 (ns)	$A_2/(A_1+A_2)$ (%)	τ_2 (ns)
0	0.3	61	2.1×10^1	39	8.9×10^1
3.0	0.4	65	2.1×10^1	35	1.4×10^2
7.7	1.3	67	8.7×10^1	33	6.0×10^2
9.4	1.9	63	1.1×10^2	37	7.7×10^2
10.0	2.8	55	1.4×10^2	45	9.7×10^2
11.9	4.5	50	2.4×10^2	50	1.5×10^3

fluorophore was confirmed to be $[Au_{23}(SCy)_{16-x}(SD2)_x]^-$ based on the similarity between the absorption and the excitation spectra (Fig. S5). The PL QYs of $[Au_{23}(SCy)_{16-x}(SD2)_x]^-$, estimated by using that of $[Au_{23}(SCy)_{16}]^-$ as a reference,[28] monotonically increased from 0.3% at x = 0 to 4.5% at x = 11.9 (Table 1). Fig. 5b shows the PL decay profiles of $[Au_{23}(SCy)_{16-x}(SD2)_x]^-$. The fitting results show that the lifetimes of the fluorescence and phosphorescence became longer with the increase in x (Table 1), due to the suppression of nonradiative decay processes in $[Au_{23}(SCy)_{16-x}(SD2)_x]^-$. Although there is no direct evidence at present, we speculate that the CH–π and/or π–π interactions between the phenyl groups in the side chains of the D2S ligands may rigidify the Au_{13} core and suppress the nonradiative decay processes. The fitting also indicates that the relative fluorescence:phosphorescence ratio changed from 6:4 to 5:5 with x (Table 1), suggesting that the D2S ligands promote intersystem crossing. In contrast, we could not evaluate the quantitative effects of D1S on the PL properties since the $[Au_{23}(SCy)_{16-x}(SD1)_x]^-$ samples were contaminated by larger Au clusters (Fig. S3). The PL spectra of the $[Au_{23}(SCy)_{16-x}(SD1)_x]^-$ samples with $x \geq 3.8$ were obviously broadened compared to that of $[Au_{23}(SCy)_{16}]^-$ (Figs. S6 and S7) due to the low-energy emission from the larger Au clusters. The three-dimensional PL spectrum of the sample containing $[Au_{23}(SCy)_{4.3}(SD1)_{11.7}]^-$ (Fig. S8) clearly shows that the low-energy PL band at ~1.2 eV originated from the photoexcitation of the larger Au clusters at ~1.5 eV.

To test the applicability of the present approach, we introduced D2SH into the well-known $[Au_{25}(SEtPh)_{18}]^-$ (PhEtSH = 2-phenylethanethiol) by the ligand exchange. The ESI mass spectra and optical absorption spectra (Figs. S9 and S10a) demonstrate the x value of $[Au_{25}(SEtPh)_{18-x}(SD2)_x]^-$ reached to 8.1 at MR = 100 without change in the size and structure. The PL intensity of $[Au_{25}(SEtPh)_{9.9}(SD2)_{8.1}]^-$ was ~2 times higher than that of unexchanged $[Au_{25}(SEtPh)_{18}]^-$ (Fig. S10b). The results suggest that this strategy can be applied to improve the PL QY of more emissive thiolate-protected Au clusters such as $Au_{22}(SG)_{18}$ (GS = glutathionate; PL QY = 8%)[29] and $Au_{24}(SCH_2Ph^tBu)_{20}$ (PL QY = 2%)[30]. The PL QY of the Au cluster core can be further enhanced by exploiting stronger CH–π and π–π interaction between higher generation ($n \geq 3$) D*n*SH or hydrogen-bonding interaction between peptide-based dendrons.[31]

In summary, we attempted to introduce dendron thiols (D*n*SH, n = 1, 2) to $[Au_{23}(SCy)_{16}]^-$ via the ligand exchange approach. Up to ~12 D2S ligands replaced the CyS ligands while retaining the atomic packing, whereas the introduction of D1S ligands partially induced the aggregation into Au_{41-46} clusters. The optical absorbance of $[Au_{23}(SCy)_{16-x}(SD2)_x]^-$ in the >2.5 eV region was increased as a function of x due to the involvement of the phenyl groups in the D2S ligands. The photoluminescence quantum yield (PL QY) of $[Au_{23}(SCy)_{16-x}(SD2)_x]^-$ was enhanced by a factor of 15 from 0.3% at x = 0 to 4.5% at x = 11.9. This remarkable enhancement of the PL QY suggests that the D2S ligands rigidify the Au_{13} core of $[Au_{23}(SCy)_{16-x}(SD2)_x]^-$ via inter-ligand CH–π and/or π–π interactions and suppress the nonradiative decay processes.

We thank Mr. Haru Hirai and Ms. Megumi Suyama for their technical support on PL measurements. The research was financially supported by the CREST program (Grant No. JPMJCR20B2) of the Japan Science and Technology Agency (JST), the Elements Strategy Initiative for Catalysts & Batteries (ESICB),

and a Grant-in-Aid for Scientific Research (Grant No. 20H00370) from the Ministry of Education, Culture, Sports, Science and Technology (MEXT) of Japan. T.O. is grateful for a research fellowship from the Japan Society for the Promotion of Science (JSPS) (Grant No. 20J13652) and the Hisao Iwai Memorial Scholarship Foundation. The synchrotron radiation experiment was performed with the approval of the Japan Synchrotron Radiation Research Institute (JASRI) (Proposal No. 2021A1220).

Conflicts of interest

There are no conflicts to declare.

Notes and references

1. D. A. Tomalia and S. N. Khanna, *Chem. Rev.*, 2016, **116**, 2705–2774.
2. K. Yamamoto, T. Imaoka, M. Tanabe and T. Kambe, *Chem. Rev.*, 2020, **120**, 1397–1437.
3. M.-K. Kim, Y.-M. Jeon, W. S. Jeon, H.-J. Kim, K. Kim, S. G. Hong and C. G. Park, *Chem. Commun.*, 2001, 667–668.
4. R. Wang, J. Yang, Z. Zheng, M. D. Carducci, J. Jiao and S. Seraphin, *Angew. Chem. Int. Ed.*, 2001, **40**, 549–552.
5. S. Nakao, K. Torigoe, K. Kon-No and T. Yonezawa, *J. Phys. Chem. B*, 2002, **106**, 12097–12100.
6. Y. Komine, I. Ueda, T. Goto and H. Fujihara, *Chem. Commun.*, 2006, 302–304.
7. T. Mizugaki, M. Murata, S. Fukubayashi, T. Mitsudome, K. Jitsukawa, K. Kaneda, *Chem. Commun.*, 2008, 241–243.
8. R. Jin, C. Zeng, M. Zhou and Y. Chen, *Chem. Rev.*, 2016, **116**, 10346–10413.
9. I. Chakraborty and T. Pradeep, *Chem. Rev.*, 2017, **117**, 8208–8271.
10. H. Hirai, S. Ito, S. Takano, K. Koyasu and T. Tsukuda, *Chem. Sci.*, 2020, **11**, 12233–12248.
11. R. Jin, *Nanoscale*, 2015, **7**, 1549–1565.
12. M. Rambukwella, N. A. Sakthivel, J. H. Delcamp, L. Sementa, A. Fortunelli and A. Dass, *Front. Chem.*, 2018, **6**, 330.
13. X. Kang and M. Zhu, *Chem. Mater.*, 2019, **31**, 9939–9969.
14. Y. Wang and T. Burgi, *Nanoscale Adv.*, 2021, **3**, 2710–2727.
15. A. Das, T. Li, K. Nobusada, C. Zeng, N. L. Rosi and R. Jin, *J. Am. Chem. Soc.*, 2013, **135**, 18264–18267.
16. Q. Li, M. Zhou, W. Y. So, J. Huang, M. Li, D. R. Kauffman, M. Cotlet, T. Higaki, L. A. Peteanu, Z. Shao and R. Jin, *J. Am. Chem. Soc.*, 2019, **141**, 5314–5325.
17. L. Zhang, F. Huo, Z. Wang, L. Wu, X. Zhang, S. Höppener, L. Chi, H. Fuchs, J. Zhao, L. Niu and S. Dong, *Langmuir*, 2000, **16**, 3813–3817.
18. D. Li and J. Li, *Colloids Surf., A*, 2005, **257–258**, 255–259.
19. M. P. Maman, A. S. Nair, H. Cheraparambil, B. Pathak and S. Mandal, *J. Phys. Chem. Lett.*, 2020, **11**, 1781–1788.
20. T. W. Ni, M. A. Tofanelli, B. D. Phillips and C. J. Ackerson, *Inorg. Chem.*, 2014, **53**, 6500–6502.
21. Y. Niihori, Y. Kikuchi, A. Kato, M. Matsuzaki and Y. Negishi, *ACS Nano*, 2015, **9**, 9347–9356.
22. A. Fernando and C. M. Aikens, *J. Phys. Chem. C*, 2015, **119**, 20179–20187.
23. C. M. Aikens, *J. Phys. Chem. Lett.*, 2010, **1**, 2594–2599.
24. A. Tlahuice-Flores, R. L. Whetten and M. Jose-Yacaman, *J. Phys. Chem. C*, 2013, **117**, 20867–20875.
25. O. Baseggio, M. De Vetta, G. Fronzoni, D. Toffoli, M. Stener, L. Sementa and A. Fortunelli, *Int. J. Quantum Chem.*, 2018, **118**, e25769.
26. S. Yamazoe, S. Takano, W. Kurashige, T. Yokoyama, K. Nitta, Y. Negishi and T. Tsukuda, *Nat. Commun.*, 2016, **7**, 10414.
27. R. Yang, D. M. Chevrier, C. Zeng, R. Jin and P. Zhang, *Can. J. Chem.*, 2017, **95**, 1220–1224.
28. K. Rurack and M. Spieles, *Anal. Chem.*, 2011, **83**, 1232–1242.
29. Y. Yu, Z. Luo, D. M. Chevrier, D. T. Leong, P. Zhang, D.-e. Jiang and J. Xie, *J. Am. Chem. Soc.*, 2014, **136**, 1246–1249.
30. Z. Gan, Y. Lin, L. Luo, G. Han, W. Liu, Z. Liu, C. Yao, L. Weng, L. Liao, J. Chen, X. Liu, Y. Luo, C. Wang, S. Wei and Z. Wu, *Angew. Chem., Int. Ed.* 2016, **55**, 11567–11571.
31. K. Isozaki, R. Ueno, K. Ishibashi, G. Nakano, H. Yin, K. Iseri, M. Sakamoto, H. Takaya, T. Teranishi and M. Nakamura, *ACS Catal.*, 2021, **11**, 13180–13187.

